CrossMark

ARTICLE

Enhanced hydrogen generation by solid-state thermal decomposition of $NaNH_2$–$NaBH_4$ composite promoted with Mg–Co–B catalyst

Ying Bai and Zi-wei Pei
Beijing Key Laboratory of Environmental Science and Engineering, School of Materials Science and Engineering, Beijing Institute of Technology, Beijing 100081, China

Feng Wu
Beijing Key Laboratory of Environmental Science and Engineering, School of Materials Science and Engineering, Beijing Institute of Technology, Beijing 100081, China; and Collaborative Innovation Center of Electric Vehicles in Beijing, Beijing 100081, China

Jian-hu Yang
Beijing Key Laboratory of Environmental Science and Engineering, School of Materials Science and Engineering, Beijing Institute of Technology, Beijing 100081, China

Chuan Wu[a)]
Beijing Key Laboratory of Environmental Science and Engineering, School of Materials Science and Engineering, Beijing Institute of Technology, Beijing 100081, China; and Collaborative Innovation Center of Electric Vehicles in Beijing, Beijing 100081, China

(Received 6 January 2017; accepted 3 February 2017)

The on-site hydrogen supply is a key issue for the commercialization of the fuel cells, which is one of the important ways for realizing a hydrogen-economy society. Composite $NaNH_2$–$NaBH_4$ is regarded as a promising high-capacity hydrogen storage material. In this paper, the composite $NaNH_2$–$NaBH_4$ (2/1) was synthesized via a solid-state ball milling method. To improve the hydrogen generation kinetics, a multiplex metal boride Mg–Co–B was selected as the catalyst. It was found that Na_3BN_2 and metal Na were byproducts in the thermal decomposed sample by X-ray diffraction analysis. Thermogravimetry and differential thermal analysis indicated that the main decomposition stages of the catalyst promoted $NaNH_2$–$NaBH_4$ material were split into three stages. The activation energy of the Mg–Co–B promoted $NaNH_2$–$NaBH_4$ (2/1) material below 300 °C was 76.4 KJ/mol, which is only 47.9% of that of the pristine $NaNH_2$–$NaBH_4$ (2/1), and implying much better hydrogen generation kinetics.

I. INTRODUCTION

The key technology to apply hydrogen energy effectively is to develop safe, economical, and efficient hydrogen storage system.[1] Hydrogen fuel cells with high energy efficiencies caught more and more attention and are expected to play important roles toward a better hydrogen-economy society. To meet the fast increasing hydrogen demand of fuel cells, mass hydrogen storage and utilization become a big challenge.[2–6] Complex hydride materials, due to their high hydrogen storage capacities, are regarded as a promising way to satisfy the urgent hydrogen supply requirements. Bogdanovic' et al.[7] observed hydrogen release and absorption for titanium-catalyzed $NaAlH_4$, which was composed firstly by Finholt[8] in 1955. Later, P. Chen et al.[9] and A. Züttel et al.[10] investigated $LiNH_2$ and $LiBH_4$ related structures and properties, respectively.[11] Futhermore, the complex light-weight hydrogen mixtures which have high gravimetric and volumetric hydrogen densities can be regarded as desirable candidates for the efficient hydrogen storage, since, comparing with single material, the problems of elevated decomposition temperature, reversibility, and impurities in the released gas can be solved through mixing hydride.[12–14] The hydrogen storage and generation performances of complex hydride materials, for instance, metal borohydrides, have been widely studied in aqueous solutions.[15–20] Recently, solid state hydrogen generation based on metal borohydrides became very attractive[21,22] because of the potential of higher hydrogen storage capacity and good operating convenience. However, the thermal decomposition kinetics of simplex metal borohydrides is not satisfied at present. Therefore, composite borohydride–amide materials,[23–28] in which different components can reduce stability each other, thus resulting in better kinetics and high hydrogen generation amount, are regarded as an alternative choice.

Contributing Editor: Xiaobo Chen
[a)]Address all correspondence to this author.
e-mail: chuanwu@bit.edu.cn
DOI: 10.1557/jmr.2017.66

https://doi.org/10.1557/jmr.2017.66 Published online by Cambridge University Press

 © Materials Research Society 2017

A new type of mixed alkali metal hydride system was proposed by F.E. Pinkerton in 2005,[29] composed of $LiNH_2$ and $LiBH_4$, forming a unique interaction, i.e., $N–H^{\delta+}/H^{\delta-}–B$, defined as the "dihydrogen bond".[30,31] The lowered hydrogen desorption temperature can be attributed to the combination of protic $H^{\delta+}$ and hydridic $H^{\delta-}$. Later, various alkali and alkaline earth metal amide−borohydride have been studied extensively, including $NaBH_4$–$NaNH_2$ system which is a promising solid hydrogen storage material.[25,32,33] However, if they are expected to be used for hydrogen fuel cells, thermal decomposition kinetics of the composite borohydride–amide materials should be improved further.

Catalyst is a good way to help overcoming the energy barrier, and thus effectively improve the kinetics. So far, metal boride catalysts, such as Co–B,[17,19,34–38] Fe–B,[39,40] Ni–Co–B[34,41] have been widely used for hydrogen generation from the hydrolysis of complex hydrides. Recent research elaborated that Co–B can also be used as a catalyst for the thermal decomposition of complex hydrides.[27] However, since cobalt is an expensive and very limited resource, low cobalt or non-cobalt catalysts are still of our concern. Furthermore, for better practical application, more metal boride catalysts have been studied. According to our previous work, in alkaline secondary batteries, Mg–Co–B[42] exhibits the similar electrochemical hydrogen storage performance as Co–B,[43] and the cobalt content of this material is much lower than that of Co–B. Inspired by this idea, it is worth researching if Mg–Co–B can play the similar role as Co–B for the thermal decomposition of $NaNH_2$–$NaBH_4$. Therefore, in this work, Mg–Co–B was used as a catalyst to improve the thermal decomposition kinetics of composite hydrogen storage material $NaNH_2$–$NaBH_4$ (2/1). Furthermore, the structure and the thermal decomposition behaviors of composite $NaNH_2$–$NaBH_4$ (2/1) were discussed. Exactly as expected, it is proven that Mg–Co–B was indeed highly effective for the help in improving the kinetics.

II. EXPERIMENTAL

A. Preparation of catalyst

The Mg–Co–B catalyst was prepared via a chemical reduction method. A typical synthesis procedure was as follows: an aqueous 0.40 mol/L $MgCl_2$ + 0.40 mol/L $CoCl_2$ co-solution was first introduced into a flask. Subsequently, an excessive $NaBH_4$ alkaline solution was pumped into the flask by stirring, whereupon a dark precipitate was produced. Thereafter, the mixture was stirred for a further half an hour to ensure the complete precipitation and removal of H_2, and the precipitate was washed with deionized water to remove the soluble ions and then vacuum-dried at 50 °C for 12 h. The as-prepared sample was designated as Mg–Co–B.

B. Preparation of catalyst promoted $NaNH_2$–$NaBH_4$ (2/1)

$NaBH_4$ (98% assay, Alfa Aesar, Haverhill, Massachusetts) and $NaNH_2$ (99% assay, Acros Organics, Pittsburgh, Pennsylvania) were used directly without pretreatment. $NaNH_2$ and $NaBH_4$ with a molar ratio of 2:1 containing 3 wt% Mg–Co–B were weighed in an argon-filled glove box and then put into a ball milling jar, as shown in Fig. 1. The ball-to-powder mass ratio is 20:1 and the stainless steel balls' diameter was 8 mm. The ball milling process was carried out in a QM-3SP2 (Nanjing NanDa Instrument Plant, Nanjing, China) planetary ball mill machine under a protection of argon atmosphere at 300 rpm, and the ball milling time was 16 h, wherein the process was paused 0.2 h after every alternative operation of 1 h. After milling for 16 h, the ball milling jar was opened and the sample was taken out in the glove box. The as-prepared sample was named as $S_{16Mg–Co–B}$. The entire operations of the samples were conducted under inert atmosphere, and all the samples and materials were stored in an argon-filled glove box ($H_2O \leq 1$ ppm, $O_2 \leq 1$ ppm; Mbraun LABSTAR8510, Mbraun InertGas-Systeme GmbH, Garching, Germany).

C. Thermal analysis

The thermogravimetry and differential thermal analysis (TG-DTA) test was conducted with a ZCT-A thermogravimetric analyser/differential thermal analyser (Beijing Jingyi High-tech Instrument, Co., Ltd., Beijing, China). 5–10 mg sample was weighed and put into a corundum crucible in the glove box and then quickly transferred into the TG-DTA instrument. High purity argon (99.999%) was served as a protective gas; the flow rate was 10 mL/min; TG range was 10 mg; DTA range was 50 UV; sampling interval was 1 s. Thus the samples were measured from room temperature to 450 °C with a heating rate of 10 °C/min.

D. Structural characterization

Crystal structures of the as-prepared samples were characterized by a Rigaku DMAX2400 X-ray diffractometer (Rigaku Corporation, Tokyo, Japan) adopting Cu K_α radiation. The tube voltage was 40 kV and the tube

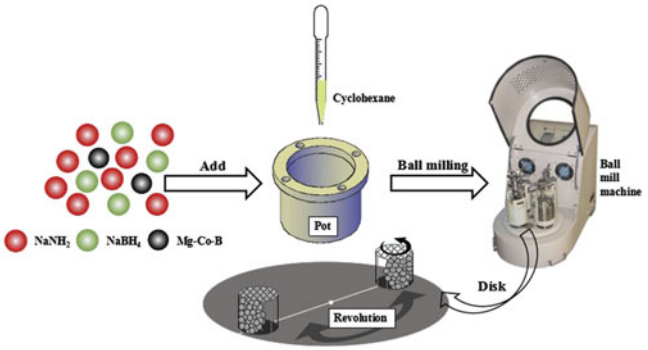


FIG. 1. Schematic illustration of the milling process.

https://doi.org/10.1557/jmr.2017.66 Published online by Cambridge University Press

current was 20 mA. The scanning range was from 10° to 80°, while the scanning rate was 8°/min.

In addition, because the hydrogen generation performance of the composite $NaNH_2$–$NaBH_4$ (2/1) samples were tested by TG-DTA, the samples used in the tests were in the milligram level, and the mass of solid products after decomposition by heating was extremely less, which was difficult to collect and detect. Therefore, to characterize structures of the decomposed samples, an alternative method was selected, namely, two grams of catalyst-promoted $NaNH_2$–$NaBH_4$ (2/1) was heated to 380 °C in a tubular furnace under the protection of argon, then being kept for 20 min, and the final product thereof was characterized by X-ray diffraction (XRD).

E. Activation energy calculation

In this paper, the activation energy was calculated by the Achar differential method, Eq. (1), and the Coats–Redfern integral method, Eq. (2), based on the thermogravimetry curves of the main temperature ranges, as described in detail in our previous work.[27] By plotting the curves of $\ln[d\alpha/dT/f(\alpha)]$ versus $1/T$ and $\ln[g(\alpha)/T^2]$ versus $1/T$, respectively, and fitting the least squares linear, the varying E, which is the slope of each straight line, can be obtained. When the E values obtained by the two methods are similar and the linear fitting correlation coefficients are of maximum value, this value is the corresponding material activation energy of the decomposition reaction,

$$\ln\left[\frac{d\alpha/dT}{f(\alpha)}\right] = \ln\left(\frac{A}{\beta}\right) - E/RT \quad , \tag{1}$$

$$\ln\left[\frac{g(\alpha)}{T^2}\right] = \ln\frac{AR}{\beta E} - E/RT \quad . \tag{2}$$

III. RESULTS AND DISCUSSION

A. XRD analysis of Mg–Co–B promoted $NaNH_2$–$NaBH_4$ (2/1)

To explore the structural characterization of the composite of Mg–Co–B doped $NaBH_4$–$NaNH_2$(1/2), we collected the sample containing 3 wt% Mg–Co–B and detected the crystal characterization via XRD measurement. Comparing the compounds with the Joint Committee on Powder Diffraction Standards (JCPDS) database including the elements Na, N, B, and H, as shown in Fig. 2, after being ball milled with the Mg–Co–B catalyst for 16 h, the composite $NaNH_2$–$NaBH_4$ (2/1) exhibits distinct peaks at $2\theta = 12.64$, 18.86, 38.09, and 43.05, which are inconsistent with the diffractions of $Na_3(NH_2)_2BH_4$ in the previous work,[26] indicating the formation of a new complex $Na_3(NH_2)_2BH_4$ phase. In addition, several characteristic peaks of $NaNH_2$ were also observed, while there is no characteristic peak of

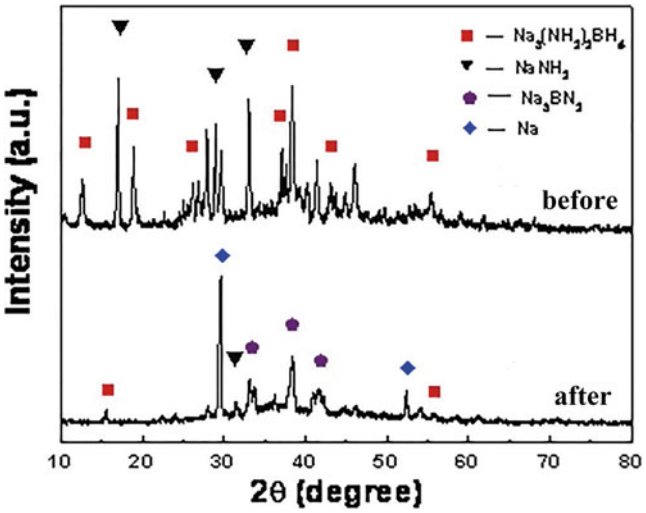


FIG. 2. XRD patterns of the sample $S_{16Mg–Co–B}$ before and after being heated at 380 °C.

$NaBH_4$ anymore. Therefore, the crystal structure of the Mg–Co–B promoted sample $S_{16Mg–Co–B}$ is very close to that of the pristine $NaNH_2$–$NaBH_4$ (2/1),[26] which implies that the Mg–Co–B catalyst has good compatibility with light-weight $NaNH_2$–$NaBH_4$, and this composite hydrogen storage system can be stably stored.

To further understand the dehydrogen performance of the novel compound $Na_3(NH_2)_2BH_4$, we heated the sample to a certain temperature. After being heated to 380 °C at a heating rate of 10 °C/min in a tubular furnace with the protection of argon, and then kept for 20 min, the sample $S_{16Mg–Co–B}$ was further detected by XRD, as shown in Fig. 2. It can be seen that the peak at $2\theta = 29.37$ is in good agreement with the strongest characteristic diffraction of metal Na, while the peaks at $2\theta = 33.47$, 38.30, 41.26 are assigned to a combination of diffractions of Na_3BN_2. Furthermore, the peak at $2\theta = 31.31$ is in agreement with the diffraction of $NaNH_2$, which is extremely weak in the XRD pattern of the sample $S_{16Mg–Co–B}$. Therefore, thermal decomposition products of $S_{16Mg–Co–B}$ comprise metal Na, Na_3BN_2, small amount of undecomposed $NaNH_2$, and without $NaBH_4$ and B.

B. TG-DTA of $S_{16Mg–Co–B}$

TG analysis and DTA were conducted simultaneously with a temperature-rising program from room temperature to 450 °C (10 °C/min). Based on the TG curve, the whole process can be roughly divided into three steps, which is in accord with the DTA curve, as shown in Fig. 3. The first stage is in the temperature range 72–210.3 °C and the second stage of degradation occurs in the range 210.3–304.6 °C, with a mass loss of 2.8 wt% in these two stages, which accounts for about 40% of the total weight loss. The third stage is in the temperature range 304.6–410 °C, and this step is a major dehydrogenation

https://doi.org/10.1557/jmr.2017.66 Published online by Cambridge University Press

process with a mass loss of 4.19 wt%. Meanwhile, three endothermic peaks at 153.3, 207, and 391 °C, as well as three exothermic peaks at 254.3, 304.8, and 354.5 °C are observed in the DTA curve. Combined with the TG curve, it is reasonable that the phase-transition temperature of $S_{16Mg\text{-}Co\text{–}B}$ is 147.6 °C and the fusion temperature of $S_{16Mg\text{–}Co\text{–}B}$ is 188.1 °C. Three exothermic peaks at 254.3, 304.8, and 354.5 °C make clear that the decomposition process of $S_{16Mg\text{–}Co\text{–}B}$ consists of three steps, after reaching its fusion temperature. Meanwhile, it demonstrates that the dehydrogenation process of the novel compound $Na_3(NH_2)_2BH_4$ is an exothermic decomposition reaction. The third endothermic peak at 391 °C means the phase-transition process of the decomposed products. Based on the above analysis, it is explicit that the main decomposition stage of Co–Mg–B promoted $NaNH_2$–$NaBH_4$ is a multi-step reaction, and the total weight loss is close to the theoretical value. Furthermore, according to the investigation of Bai,[26] the peak temperature with the maximal decomposition rate of the solid ball-milling product is 346.2 °C, which is higher than 254.3 °C of the corresponding peak temperature of the sample $S_{16Mg\text{–}Co\text{–}B}$, comparing the varying composite $NaNH_2$–$NaBH_4$ (2/1) systems. It can be concluded that the thermal stability of the composite hydrogen storage material with the catalyst Co–Mg–B is further reduced and the dehydrogen thermodynamic performance is efficiently improved.

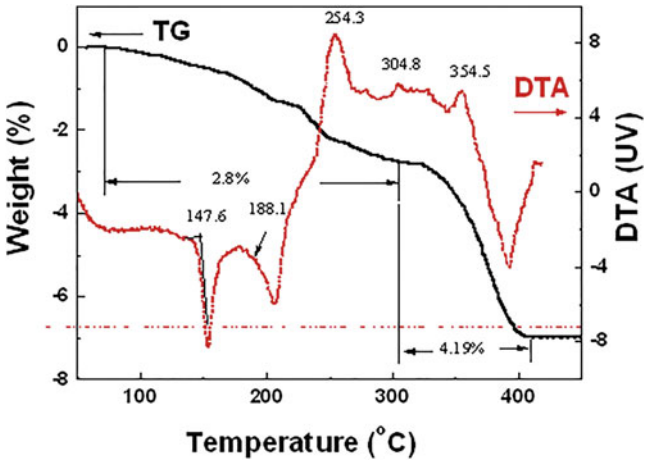


FIG. 3. The TG-DTA curves of the sample $S_{16Mg\text{–}Co\text{–}B}$.

C. Kinetics of Mg–Co–B-promoted $NaNH_2$–$NaBH_4$ (2/1)

From the TG curve, it can be seen that below 300 °C, the weight loss curve is relatively flat, and the weight loss rate is very sharp, which indicates that the activation energy of this stage may be relatively low. The decomposition reaction of 3 wt% Mg–Co–B promoted $NaNH_2$–$NaBH_4$ (2/1) occurs in two main stages, which are 72–304.6 °C and 304.6–410 °C, as shown in Fig. 3. The temperatures of conversion rate α from 0.1 to 0.9 were obtained from the TG curve, and the activation energies were calculated with these 32 kinetic functions

TABLE I. Kinetic data of the sample $S_{16Mg\text{–}Co\text{–}B}$ at the first thermal decomposition stage of 72–304.6 °C.

Conversion rate α	T/K	$d\alpha/dT$	$f(\alpha)$	$g(\alpha)$	$\ln\left[\frac{d\alpha/dT}{f(\alpha)}\right]$	$\ln\left[\frac{g(\alpha)}{T^2}\right]$	$1/T$
0.1	438.4768	0.0656	41.96489	0.001164	−6.46101	−18.9225	0.00162
0.2	455.122	0.0509	19.42569	0.004893	−5.94449	−17.5611	0.001595
0.3	477.0659	0.0517	11.88139	0.011626	−5.43727	−16.7898	0.001573
0.4	492.4267	0.0804	8.080542	0.021955	−4.6102	−16.2175	0.001559
0.5	503.5592	0.0947	5.770983	0.036706	−4.10988	−15.7482	0.001547
0.6	514.0495	0.0954	4.199225	0.057116	−3.78458	−15.3473	0.001535
0.7	525.1285	0.0832	3.037657	0.085193	−3.59759	−14.9901	0.001526
0.8	539.0976	0.0609	2.112748	0.124671	−3.54651	−14.6619	0.001516
0.9	559.2753	0.0422	0.434294	0.669741	−3.42719	−14.3431	0.001502

TABLE II. Kinetic data of the sample $S_{16Mg\text{–}Co\text{–}B}$ at the second thermal decomposition stage of 304.6–410 °C.

Conversion rate α	T/K	$d\alpha/dT$	$f(\alpha)$	$g(\alpha)$	$\ln\left[\frac{d\alpha/dT}{f(\alpha)}\right]$	$\ln\left[\frac{g(\alpha)}{T^2}\right]$	$1/T$
0.1	617.4396	0.0995	41.964887	0.001164	−6.04443	−19.6071	0.00162
0.2	627.0135	0.0924	19.425687	0.004893	−5.34822	−18.2019	0.001595
0.3	635.5941	0.1576	11.881388	0.011626	−4.32267	−17.3636	0.001573
0.4	641.246	0.1871	8.0805425	0.021955	−3.76557	−16.7456	0.001559
0.5	646.5125	0.1907	5.7709832	0.036706	−3.4099	−16.248	0.001547
0.6	651.368	0.2298	4.1992246	0.057116	−2.90545	−15.8208	0.001535
0.7	655.4271	0.2556	3.0376573	0.085193	−2.47523	−15.4334	0.001526
0.8	659.4862	0.2240	2.1127476	0.124671	−2.2441	−15.065	0.001516
0.9	665.8317	0.0951	1.2993373	0.184557	−2.61468	−14.6919	0.001502

https://doi.org/10.1557/jmr.2017.66 Published online by Cambridge University Press

of 32 diverse mechanisms. The kinetic data of the sample $S_{16Mg–Co–B}$ at the major thermal decomposition stages are listed in Tables I and II, respectively. And the activation energies of the two stages calculated by Ginstling–Brounstein function are 76.4 KJ/mol and 349.8 KJ/mol, respectively, as shown in Figs. 4 and 5.

The detailed equation derivation and the data analysis method were published in our previous work.[27] Therefore, compared with the activation energy of the pristine $NaNH_2$–$NaBH_4$ (2/1), namely, 159.6 KJ/mol,[27] that of the sample $S_{16Mg–Co–B}$ becomes rather lower below 304.6 °C, which indicates that the Mg–Co–B catalyst works highly efficiently in the low temperature range. Of course, for practical utilization, the hydrogen yield in the low temperature range still needs to be improved.

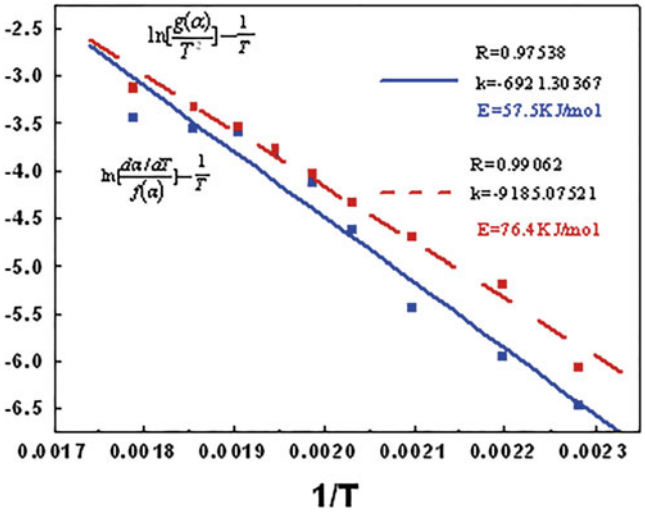


FIG. 4. Linear fitted plots of the data originated from the Ginstling–Brounshtein equation for the sample $S_{16Mg–Co–B}$ at the first thermal decomposition stage of 72–304.6 °C.

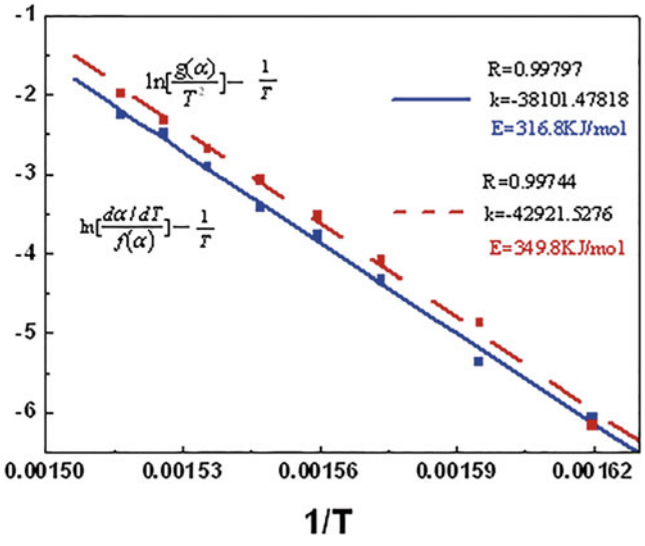


FIG. 5. Linear fitted plots of the data originated from the Ginstling-Brounshtein equation for the sample $S_{16Mg–Co–B}$ at the second thermal decomposition stage of 304.6–410 °C.

D. Catalytic mechanism of Mg–Co–B-promoted $NaNH_2$–$NaBH_4$ (2/1)

The Mg–Co–B catalyst investigated in this study has a similar structure as that of Co–B, which is a kind of amorphous alloy. The amorphous alloy, with a short-range ordered and long-range disordered structure, is totally different from the crystal metal in the array of atoms. There are many vacant electron orbits and unsaturated coordination sites on the surface of the Mg–Co–B catalyst. The reasons of the modification after being doped with the Mg–Co–B catalyst are the following: (1) H^- of BH_4^- loses electrons easily and Mg–Co–B speeds up the process of losing electrons, while the H atoms losing the electrons combine and generate H_2. (2) B unoccupied orbital and the N lone electron pair establish the donor–acceptor attraction to each other, which promotes the extrusion of H in NH_2^-, then form H_2. Finally, Na, B, N recombine and generate Na_3BN_2, as shown in Fig. 6. We conclude that the specific amorphous alloy structure of the Mg–Co–B catalyst can effectively accelerate the formation of H_2.

Moreover, we conclude the possible functions of Mg in the ternary Mg–Co–B catalyst as follows: (1) Cobalt is an expensive and very limited resource; low cobalt or non-cobalt catalysts are of our concern. And Mg metal has a low price. (2) The electronic structure of magnesium element and cobalt element is similar since the number of electrons in their outer shell is two. Therefore, Mg–Co–B can play the similar role as Co–B for the thermal decomposition of $NaNH_2$–$NaBH_4$. Moreover, the substitution of metal magnesium for partial cobalt intensifies the amorphous alloy structure of short-range ordered and long-range disordered. And the Mg–Co–B alloys are amorphous or crystalline compounds, rather than simple mixtures of metallic elements.[42] (3) With increasing heat-treating temperature, both the Mg–Co–B and Co–B precursors change from an amorphous phase to a mixture

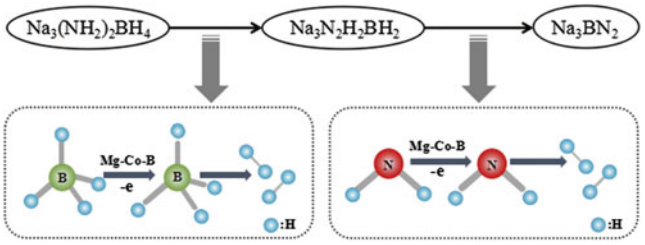


FIG. 6. Schematic diagram of the catalytic mechanism of $NaNH_2$–$NaBH_4$ (2/1) decomposition promoted by the Mg–Co–B catalyst.

https://doi.org/10.1557/jmr.2017.66 Published online by Cambridge University Press

which includes CoB. In the previous study,[17] we concluded that CoB is the key component for accelerating the reaction. We deduce that the Mg–Co–B alloys can decompose to CoB at a lower temperature.

IV. CONCLUSIONS

In summary, the corresponding influences of the Mg–Co–B catalyst on the thermal decomposition behaviors of $NaNH_2$–$NaBH_4$ (2/1) based light-weight hydrogen storage material were evaluated and discussed. According to the thermal analysis, the activation energy of Mg–Co–B promoted $NaNH_2$–$NaBH_4$ (2/1) was calculated by the Ginstling–Brounstein function. It is notable that the kinetics of $NaNH_2$–$NaBH_4$ (2/1) is effectively promoted by the Mg–Co–B catalyst. Namely, when the temperature is lower than 300 °C, $NaNH_2$–$NaBH_4$ (2/1) with the Mg–Co–B catalyst achieves a low activation energy of 76.4 KJ/mol, which implies that the composite metal boride Mg–Co–B is helpful to accelerate the thermal decomposition in the low temperature range. Therefore, hydrogen supply strategy based on the $NaNH_2$–$NaBH_4$ (2/1) composite with the Mg–Co–B catalyst is promising for low temperature fuel cell applications.

ACKNOWLEDGMENTS

The present work is supported by the National Natural Science Foundation of China (Grant No. 21476027) and Program for New Century Excellent Talents in University (Grant No. NCET-13-0033).

REFERENCES

1. X. Liu, C. Wu, F. Wu, and Y. Bai: Light metal complex hydride hydrogen storage systems. *Prog. Chem.* **27**, 1167–1181 (2015).
2. Y. Nagar, A. Schechter, B. Ben-Moshe, and N. Shvalb: Modeling the mechanical behavior of sodium borohydride ($NaBH_4$) powder. *Mater. Des.* **108**, 240–249 (2016).
3. U.B. Demirci, O. Akdim, and P. Miele: Ten-year efforts and a no-go recommendation for sodium borohydride for on-board automotive hydrogen storage. *Int. J. Hydrogen Energy* **34**, 2638–2645 (2009).
4. N.A.A. Rusman and M. Dahari: A review on the current progress of metal hydrides material for solid-state hydrogen storage applications. *Int. J. Hydrogen Energy* **41**, 12108–12126 (2016).
5. R.A. Varin, D.K. Mattar, A.S. Bidabadi, and M. Polanski: Synthesis of amorphous manganese borohydride in the ($NaBH_4$–$MnCl_2$) system, its hydrogen generation properties and crystalline transformation during solvent extraction. *J. Energy Chem.*, 1–11 (2016).
6. F. Morelle, L.H. Jepsen, T.R. Jensen, M. Sharma, H. Hagemann, and Y. Filinchuk: Reaction pathways in $Ca(BH_4)_2$−$NaNH_2$ and $Mg(BH_4)_2$−$NaNH_2$ hydrogen-rich systems. *J. Phys. Chem. C* **120**, 8428–8435 (2016).
7. B. Bogdanović and M. Schwickardi: Ti-doped alkali metal aluminium hydrides as potential novel reversible hydrogen storage materials. *J. Alloys Compd.* **253–254**, 1–9 (1997).
8. A.E. Finholt, E.C. Jacobson, A.E. Ogard, and P. Thompson: Organic reductions by sodium aluminum hydride. *J. Am. Chem. Soc.* **77**, 4163 (1955).
9. P. Chen, Z.T. Xiong, J.Z. Luo, J.Y. Lin, and K.L. Tan: Interaction of hydrogen with metal nitrides and imides. *Nature* **420**, 302–304 (2002).
10. A. Züttel, S. Rentsch, P. Fischer, P. Wenger, P. Sudan, P. Mauron, and C. Emmenegger: Hydrogen storage properties of $LiBH_4$. *J. Alloys Compd.* **356**, 515–520 (2003).
11. M.B. Ley, L.H. Jepsen, Y. Lee, Y.W. Cho, J.M.B.V. Colbe, M. Dornheim, M. Rokni, J.O. Jensen, M. Sloth, Y. Filinchuk, J.E. Jørgensen, F. Besenbacher, and T.R. Jensen: Complex hydrides for hydrogen storage-new perspectives. *Mater. Today* **17**, 122–128 (2014).
12. P. Schouwink, V. D'Anna, M.B. Ley, L.M.L. Daku, B. Richter, T.R. Jensen, H. Hagemann, and R. Černý: Bimetallic borohydrides in the system $M(BH_4)_2$−KBH_4 (M = Mg, Mn): On the structural diversity. *J. Phys. Chem. C* **116**, 10829−10840 (2012).
13. M.B. Ley, D.B. Ravnsbæk, Y. Filinchuk, Y-S. Lee, R. Janot, Y.W. Cho, J. Skibsted, and T.R. Jensen: $LiCe(BH_4)_3Cl$, a new lithium-ion conductor and hydrogen storage material with isolated tetranuclear anionic clusters. *Chem. Mater.* **24**, 1654−1663 (2012).
14. D.B. Ravnsbaek, L.H. Sørensen, Y. Filinchuk, F. Besenbacher, and T.R. Jensen: Screening of metal borohydrides by mechanochemistry and diffraction. *Angew. Chem.* **51**, 3582−3586 (2012).
15. C. Wu, H.M. Zhang, and B.L. Yi: Hydrogen generation from catalytic hydrolysis of sodium borohydride for proton exchange membrane fuel cells. *Catal. Today* **93–95**, 477–483 (2004).
16. Y. Kojima, Y. Kawai, M. Kimbara, H. Nakanishi, and S. Matsumoto: Hydrogen generation by hydrolysis reaction of lithium borohydride. *Int. J. Hydrogen Energy* **29**, 1213–1217 (2004).
17. C. Wu, F. Wu, Y. Bai, B.L. Yi, and H.M. Zhang: Cobalt boride catalysts for hydrogen generation from alkaline $NaBH_4$ solution. *Mater. Lett.* **59**, 1748–1751 (2005).
18. Y. Bai, C. Wu, F. Wu, and B.L. Yi: Carbon-supported platinum catalysts for on-site hydrogen generation from $NaBH_4$ solution. *Mater. Lett.* **60**, 2236–2239 (2006).
19. C. Wu, Y. Bai, F. Wu, B.L. Yi, and H.M. Zhang: Highly active cobalt-based catalysts in situ prepared from CoX_2 (X = Cl^-, NO_3^-) and used for promoting hydrogen generation from $NaBH_4$ solution. *Int. J. Hydrogen Energy* **35**, 2675–2679 (2010).
20. S.C. Li and F.C. Wang: The development of a sodium borohydride hydrogen generation system for proton exchange membrane fuel cell. *Int. J. Hydrogen Energy* **41**, 3038–3051 (2016).
21. A. Züttel, P. Wenger, S. Rentsch, P. Sudan, P. Mauron, and C. Emmenegger: $LiBH_4$ a new hydrogen storage material. *J. Power Sources* **118**, 1–7 (2003).
22. C.J. Lee and T. Kim: Hydrogen supply system employing direct decomposition of solid-state $NaBH_4$. *Int. J. Hydrogen Energy* **40**, 2274–2282 (2015).
23. P. Chen, Z.T. Xiong, G.T. Wu, Y.F. Liu, J.J. Hu, and W.F. Luo: Metal–N–H systems for the hydrogen storage. *Scr. Mater.* **56**, 817–822 (2007).
24. P.A. Chater, P.A. Anderson, J.W. Prendergast, A. Walton, V.S.J. Mann, D. Book, B. David, W.I.F. David, S.R. Johnson, and P.P. Edwards: Synthesis and characterization of amide-borohydrides: New complex light hydrides for potential hydrogen storage. *J. Alloys Compd.* **446–447**, 350–354 (2007).
25. M. Somera, S. Acar, C. Koz, I. Kokal, P. Höhn, R. Cardoso-Gil, U. Aydemir, and L. Akselrud: α- and β-$Na_2[BH_4][NH_2]$: Two modifications of a complex hydride in the system $NaNH_2$–$NaBH_4$: Syntheses, crystal structures, thermal analyses, mass and vibrational spectra. *J. Alloys Compd.* **491**, 98–105 (2010).

https://doi.org/10.1557/jmr.2017.66 Published online by Cambridge University Press

26. C. Wu, Y. Bai, J.H. Yang, F. Wu, and F. Long: Characterizations of composite $NaNH_2$–$NaBH_4$ hydrogen storage materials synthesized via ball milling. *Int. J. Hydrogen Energy* **37**, 889–893 (2012).
27. Y. Bai, C. Wu, F. Wu, L.L. Zhao, J.H. Yang, F. Long, and B.L. Yi: Thermal decomposition kinetics of light-weight composite $NaNH_2$–$NaBH_4$ hydrogen storage materials for fuel cells. *Int. J. Hydrogen Energy* **37**, 12973–12979 (2012).
28. Y. Bai, L.L. Zhao, Y. Wang, X. Liu, F. Wu, and C. Wu: Light-weight $NaNH_2$–$NaBH_4$ hydrogen storage material synthesized via liquid phase ball milling. *Int. J. Hydrogen Energy* **39**, 13576–13582 (2014).
29. F.E. Pinkerton, G.P. Meisner, and M.S. Meyer: Hydrogen desorption exceeding ten weight percent from the new quaternary hydride $Li_3BN_2H_8$. *J. Phys. Chem. B* **109**, 6–8 (2005).
30. Z. Huang and T. Autrey: Boron–nitrogen–hydrogen (BNH) compounds: Recent developments in hydrogen storage, applications in hydrogenation and catalysis, and new syntheses. *Energy Environ. Sci.* **5**, 9257–9268 (2012).
31. T. Richardson, S. de Gala, R.H. Crabtree, and P.E.M. Siegbahn: Unconventional hydrogen bonds: Intermolecular B–H···H–N interactions. *J. Am. Chem. Soc.* **117**, 12875–12876 (1995).
32. X.B. Yu, Y.H. Guo, D.L. Sun, Z.X. Yang, A. Ranjbar, Z.P. Guo, H.K. Liu, and S.X. Dou: A combined hydrogen storage system of $Mg(BH_4)_2$–$LiNH_2$ with favorable dehydrogenation. *J. Phys. Chem. C* **114**, 4733–4737 (2010).
33. H.L. Chu, Z.T. Xiong, G.T. Wu, J.P. Guo, X.L. Zheng, H. Teng, C.Z. Wu, and P. Chen: Hydrogen storage properties of $Ca(BH_4)_2$–$LiNH_2$ system. *Chem.–Asian J.* **5**, 1594–1599 (2010).
34. D.Y. Xu, H.Z. Wang, Q.J. Guo, and S.F. Ji: Catalytic behavior of carbon supported Ni–B, Co–B and Co–Ni–B in hydrogen generation by hydrolysis of KBH_4. *Fuel Process. Technol.* **92**, 1606–1610 (2011).
35. Y. Wang, T.L. Li, S.C. Bai, K.Z. Qi, Z.Q. Cao, K. Zhang, S.W. Wu, and D. Wang: Catalytic hydrolysis of sodium borohydride via nanostructured cobalt–boron catalysts. *Int. J. Hydrogen Energy* **41**, 276–284 (2016).
36. B.C. Weng, F.H. Xu, Z. Wu, and Z.L. Li: Hydrogen generation from $LiBH_4$ solution catalyzed by multiwalled carbon nanotubes supported Co–B nanocatalysts for a portable micro proton exchange membrane fuel cell application. *Int. J. Hydrogen Energy* **39**, 14942–14948 (2014).
37. S.S. Muir, Z.G. Chen, B.J. Wood, L.Z. Wang, G.Q. (Max) Lu, and X.D. Yao: New electroless plating method for preparation of highly active Co–B catalysts for $NaBH_4$ hydrolysis. *Int. J. Hydrogen Energy* **39**, 414–425 (2014).
38. O.V. Netskina, A.M. Ozerova, O.V. Komova, G.V. Odegova, and V.I. Simagina: Hydrogen storage systems based on solid-state $NaBH_4/Co_xB$ composite: Influence of catalyst properties on hydrogen generation rate. *Catal. Today* **245**, 86–92 (2015).
39. C. Wu, Y. Bai, and F. Wu: Fast hydrogen generation from $NaBH_4$ solution accelerated by ferric catalysts. *Mater. Lett.* **62**, 4242–4244 (2008).
40. T.N. Tuan, Y.M. Yi, J.K. Lee, and J. Lee: Fe–B catalyst fabricated by hybrid capacitive adsorption–chemical reduction method and its application for hydrogen production from $NaBH_4$ solution. *Catal. Today* **216**, 240–245 (2013).
41. C. Wu, Y. Bai, D.X. Liu, F. Wu, M.L. Pang, and B.L. Yi: Ni–Co–B catalyst-promoted hydrogen generation by hydrolyzing $NaBH_4$ solution for in situ hydrogen supply of portable fuel cells. *Catal. Today* **170**, 33–39 (2011).
42. C. Wu, Y. Bai, F. Wu, X. Wang, J.Y. Lu, and C. Qiao: Novel ternary metal boride Mg–Co–B alloys as anode materials for alkaline secondary batteries. *Electrochem. Commun.* **11**, 2173–2176 (2009).
43. C. Wu, Y. Bai, F. Wu, L.W. Dong, X. Wang, L.X. Yang, and C.Z. Zhang: Structural evolutions and electrochemical behaviors of Co–B alloys as anode materials for alkaline secondary batteries. *Electrochim. Acta* **53**, 4715–4720 (2008).

https://doi.org/10.1557/jmr.2017.66 Published online by Cambridge University Press